Supporting Material

Smooth DNA Transport Through a Narrowed Pore Geometry

Spencer Carson[1], Jim Wilson[2], Aleksei Aksimentiev[2], and Meni Wanunu[1,3†]

[†]Email: wanunu@neu.edu

SM-1: *Materials and Methods*

Nanopore experiments. Substrates for our solid-state nanopore membranes were formed by the thermal oxidation of silicon <100> wafers to generate a ~2.5-μm thick SiO_2 dielectric barrier layer. Following oxidation, low-pressure chemical vapor deposition is used to deposit a 45-nm-thick low-stress silicon nitride layer. Using a combination of photolithography and dry/wet etching steps, a wafer was etched to obtain an array of 5x5 mm^2 chips with freestanding square membranes at their centers (10-50 μm in length), and further thinned to ~25 nm using a controlled reactive ion etch process. A transmission electron microscope (JEOL 2010FEG) at high energy (200 kV) and magnification (1.5 Mx) was then used to "drill" nanopores of measureable shape and diameters in the range of 2-10 nm. Due to various factors we have found that our effective nanopore diameters did not always correspond to the TEM-based diameter, so all quoted pore diameters in the paper were estimated from ion current measurements using a solitary model in which the effective thickness is 1/3 of the total membrane thickness (see **SM-4**).(1, 2)

Prior to conducting a nanopore experiment the nanopore chips were cleaned by a 10-minute immersion in a fresh heated piranha solution (1:2 mixture of H_2O_2 and H_2SO_4), followed by cooling and a copious rinse with water. The chips were then stored in DI water until an experiment was carried out. Upon use, the chips were vacuum dried and mounted on a gasket-sealed two-chamber cell, each equipped with an electrode that is connected to a high-bandwidth amplifier. Buffered electrolyte (0.4 M KCl, buffered to pH 7.9 using 10 mM Tris and 1 mM EDTA) was added to both chambers, and the pore was evaluated by conductance measurements and by recording a time-stable DC ion current response for nonzero bias.

Molecular dynamics simulations. A custom tclforces script was used to produce DNA displacement. Each phosphorous atom of DNA was harmonically restrained (k_z = 69.5 or 6.9 pN/Å) to an individual template particle. The z coordinates of the template particles were synchronously changed according to the target DNA velocity. The initial coordinates of the template particles were that of B-form DNA. In addition to the above pulling restraints, the phosphorous atoms of the DNA were harmonically restrained (k_{rad} = 69.5 pN/Å) to a cylindrical

shell coaxial with the pore. Under such restraints, the DNA fragment could rotate about its axis but not stretch or move away from the center of the pore. In each production simulation, the DNA was pulled 3.4 nm through the nanopore. Three pulling velocities were used: 0.1133 nm/ns, 0.0567 nm/ns, and 0.0283 nm/ns, requiring 30, 60, and 120 ns simulation, respectively. Five independent simulations were carried out for each pulling velocity; five additional simulations were done for the 4.5 nm nanopore, where thermal fluctuations were more significant. The instantaneous force applied to all phosphorous atoms was recorded every 200 fs. The time average of the instantaneous force was used to determine the diffusion constant.

Bootstrapping and fit optimization. We estimated D and v using a numerical maximum-likelihood procedure. We first eliminated any dwell time data points that were caused by fast collision events or falsely detected by our analysis software by setting a minimum and maximum threshold for dwell time. After these limits were incorporated, standard errors for D and v were estimated by bootstrapping. For each experimental dataset, we created 10,000 bootstrap samples by resampling from the original data with replacement. The estimates of D and v generated from these resampled datasets formed bootstrap distributions for D and v. The distributions were approximately Gaussian, so we report the standard deviation of each bootstrap distribution as a standard error for the corresponding parameter estimate.

SM-2: *Effect of low-pass filter frequencies on event detection*

Many nanopore experiments are conducted with high salt conditions (i.e., > 1 M KCl or other electrolytic salt), which boosts the ionic current and reduces the relative amplitude of thermal and capacitive noise.(3, 4) Since our experiments use an ionic concentration of 0.4 M KCl we need to take great care in deciding what low-pass filter to apply when analyzing our experimental data. Many factors, such as desired time resolution and signal noise, must be taken into consideration when determining what filtering should be done on nanopore current traces. The low-pass filter selected can also change the number and types of events detected based on the current amplitude ΔI of each respective event. As a demonstration of this effect, in **Fig. S1** we have plotted a sample 2-second current trace from an experiment for 100 bp after applying a filter of 10 kHz (*black*) and 200 kHz (*green*). All translocation events, signified by deeper current blockades, are detected for both filters, but a few collision events are only detected by the 10 kHz filter (*designated by red ovals*).

Since these collisions are masked by the noise when filtering at 200 kHz, we effectively sift out undesirable events by simply increasing our filter frequency without the need of additional manual analysis.

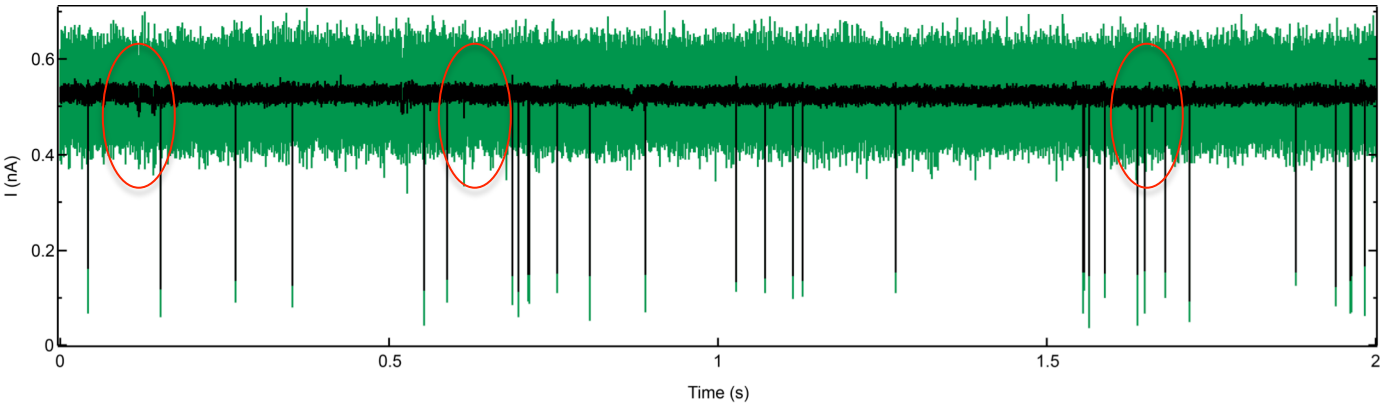

FIGURE S1 Effect of signal bandwidth on masking DNA collision spikes. A two-second example current trace for 100 bp DNA (V = 200 mV, d = 2.9 nm) is low-pass filtered to 10 kHz (*black*) and 200 kHz (*green*). As seen by the red ovals, collisions of DNA with the pore, which yielded low-amplitude spikes, are missed by our event analysis routine, which was performed on data low-pass filtered at 200 kHz.

SM-3: *Time stability and pore-to-pore reproducibility of DNA translocation*

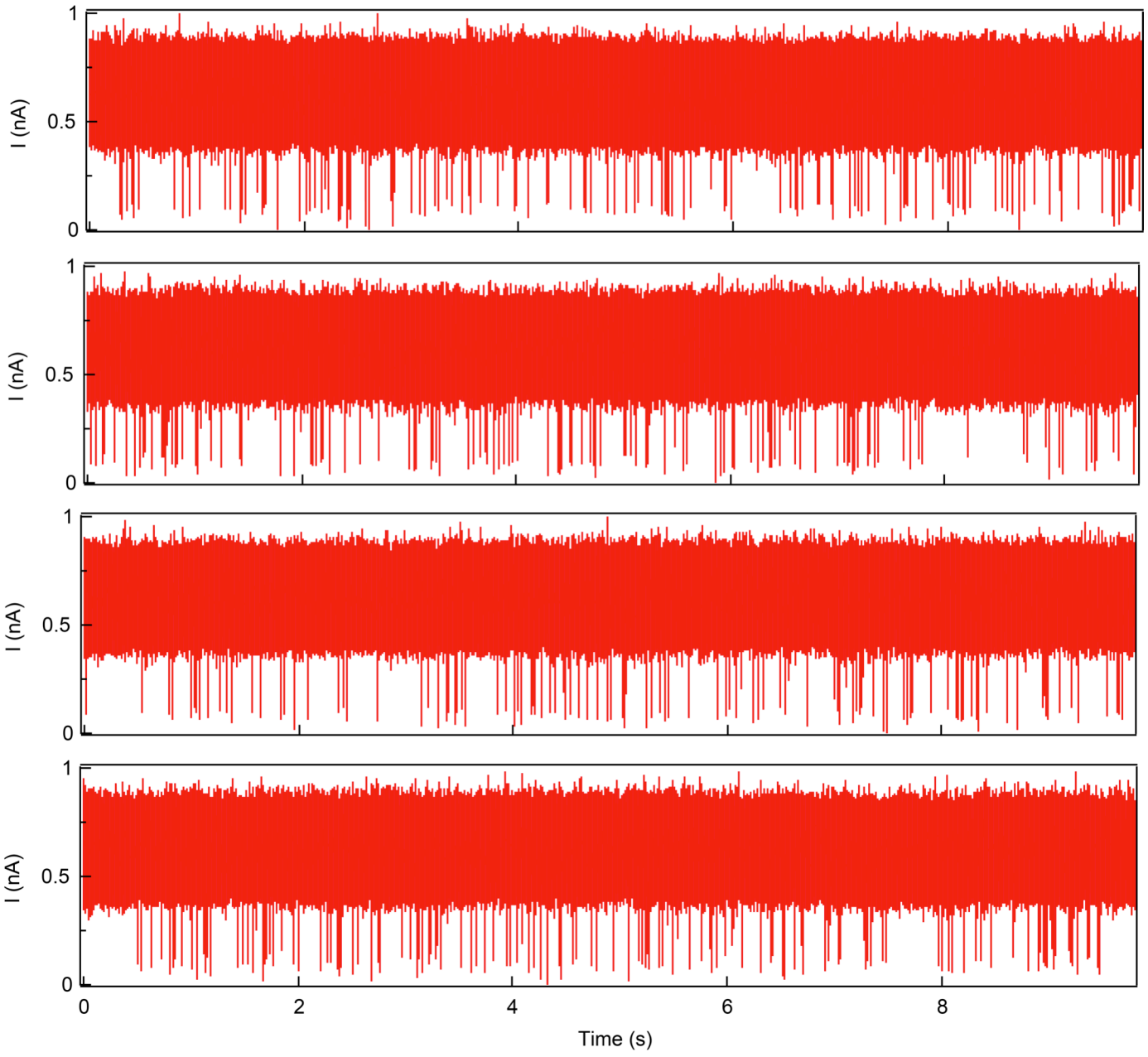

FIGURE S2 A representative, continuous 40-second current trace for 500 bp transport at V = 200 mV through a pore of d = 3.0 nm (raw data downsampled to 500 kHz and low-pass filtered at 200 kHz). The vast majority of events show great uniformity in both dwell time t_d and current blockade ΔI.

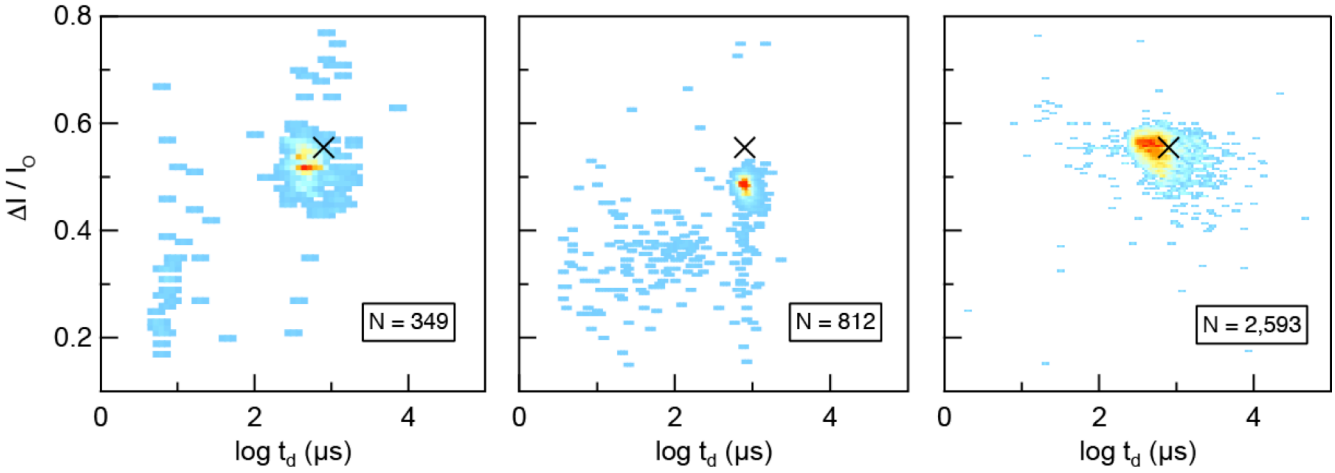

FIGURE S3 Contour plots of 500 bp DNA translocation at V = 200 mV for three different pores with d = 2.8 – 3.0 nm and similar thickness (b_{eff} = 8 – 10 nm). Each experiment yielded a mean dwell time in the range of 600-900 μs, demonstrating nice reproducibility in our nanopores. The X marker on each plot designates the mean dwell time and fractional current blockade of the dataset with the greatest number of events (*right panel*).

SM-4: *Determination of pore diameter and thickness based on open and blocked pore ionic current (I_o and I_b)*

To estimate the size any nanopore (diameter and thickness), we used the following nanopore conductance model:(5)

$$I = \sigma V \left(\frac{4 b_{eff}}{\pi d^2} + \frac{1}{d} \right)^{-1} \qquad \text{(S1)}$$

The first term inside the parentheses represents the classical geometrical contribution to the resistance due to the length and diameter of the nanopore ($R \sim b_{eff}/d^2$). The second term is known as the access resistance, which dominates as $b_{eff} \to 0$ and prevents the resistance from becoming zero in this limit.(6, 7) We first analyzed our current traces to determine the open pore current I_o and the blocked pore current I_b for a given pore. With these two quantities, along with the known applied

voltage V and the solution conductance σ (~50 mS/cm for 0.4 M KCl), it is possible to solve this conductance model numerically to estimate the pore diameter d and the effective membrane thickness b_{eff} for any experiment. Since the nanopores that we fabricated by TEM drilling are hourglass shaped, it has been determined experimentally that it is most accurate to model the membrane using one-third of the total thickness, also known as the effective thickness b_{eff}.(1, 2) Fitting our current data to this model also served as a useful confirmation of the diameter we estimated from our TEM images. Any pore diameter cited in this paper is the value determined experimentally using Eq. S1.

SM-5: *Determination of fit percentage using the 1D drift-diffusion model*

When using the 1D drift-diffusion model described in the main text, we constrained the fit to a specific thickness b, which was calculated using **Eq. S1** and the known DNA length ($b = b_{eff} + L_C$). Using this thickness constraint we obtained values for D and v when fitting our model to each dwell time distribution. The percentage of dwell time data that is beneath the fitting function was determined by an integration method, which estimates what fraction of our data is contained by the fit. This method was assisted by using an automated integration function in Igor Pro (WaveMetrics, Inc., Portland, OR), which computes the cumulative area integral of both the dwell time histogram and the fitting function over the entire time range of the data. By aligning these two cumulative area curves on the same plot, the percentage of events that agree with our model can be determined. This is accomplished by finding the dwell time where the experimental curve deviates from the fit curve, then dividing the area corresponding to this dwell time by the total area of the experimental histogram, which yields a fractional value representing the fit percentage. When using this method we also made certain to exclude events that occur at fast time scales outside of the fit.

SM-6: *Derivation of axial diffusion coefficient* $\mathbf{D_A}$

When extracting diffusion coefficients from our dwell time distributions, we relate this to a bulk value of D_o for 75 bp, or one-half of a persistence length for dsDNA. Approximating DNA as a short rod-like molecule, the bulk diffusion coefficient D_o can be broken down into its axial and radial components, D_A and D_R. Since our model is one-dimensional and we are interested in the DNA

translocation trajectory, only the axial component of the diffusion D_A is relevant. By ignoring end-effects of the molecule, the axial component can be approximated as $D_A \sim 2D_R$.(8) Using this relationship and the fact that $D_o = (D_A + 2D_R)/3$,(9) we solve for D_A to obtain $D_A = 3/2\ D_o$. For notational simplicity, D_A is referred to as D in the main article.

SM-7: *Finite-element simulations of DNA nanopore translocation*

As shown in **Fig. S4**, we modeled our experimental setup as two cylindrical compartments, each with a diameter of 12 µm and a height of 10 µm, connected by an hourglass shaped nanopore. By defining our geometry in this way, we have assumed that our membrane is a perfect electrical insulator, which is an acceptable simplification for materials such as SiN_x. The two important user-defined parameters for the nanopore geometry are the diameter d and the effective membrane thickness b_{eff}, which defines the total membrane thickness (i.e., $3b_{eff}$) and is used to construct the hourglass shape of the pore. The diameter of the pore opening was defined as $2.5d$, which yielded an

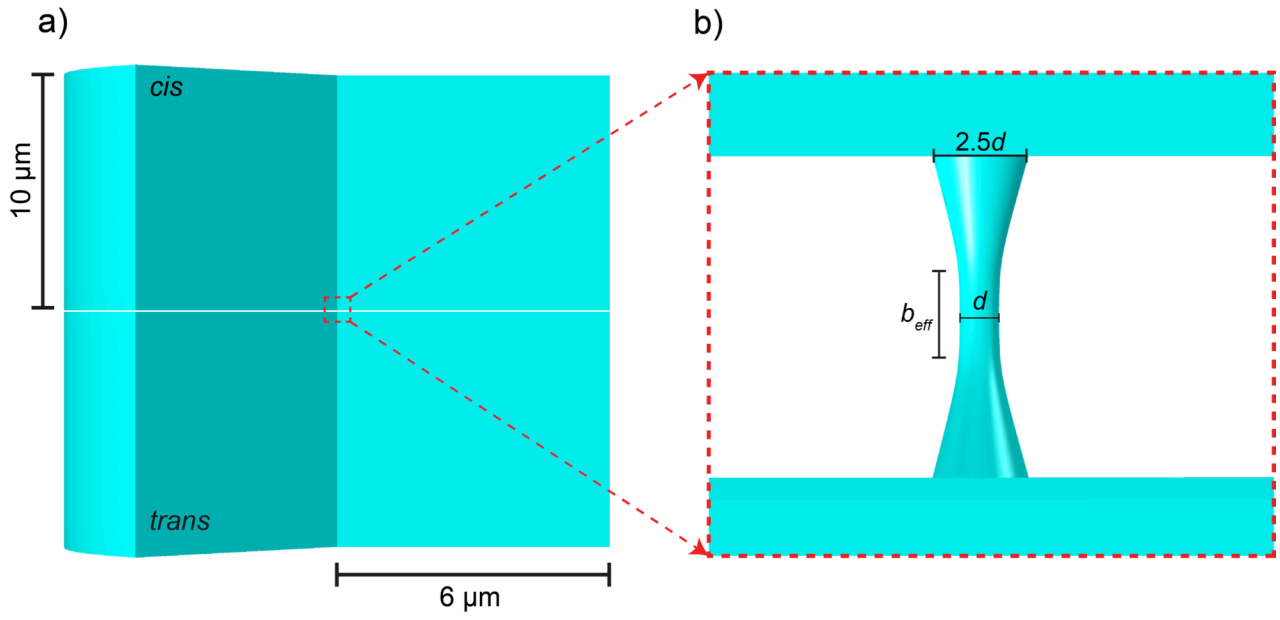

FIGURE S4 Finite element simulation details. (***a***) An illustration of our custom simulation geometry with two cylindrical compartments (*cis* and *trans*) connected by a nanoscale pore. (***b***) An enlarged view of the hourglass-shaped nanopore that joins the two chambers across an insulating membrane (*white region*). The notable variables of diameter d and effective pore length b_{eff} are the most crucial when defining our pore geometry. As noted in the main text, b_{eff} is simply taken to be one-third of the total membrane thickness.

hourglass shape reasonably consistent with TEM imaging previously reported.(2) Whenever DNA was added to the geometry of the simulation (**Fig. 5, *b*** and ***d***) it was modeled as an insulating cylinder with a diameter of 2.2 nm and height of 80 nm. We defined our mesh to be much finer inside and in the vicinity of the nanopore (meshing elements as small as 0.1 nm), and then used normal meshing settings for the rest of the geometry (elements > 1 nm). We also added boundary layers to our mesh at the edges of the nanopore, which will dampen any adverse effects of the sharp edges at the pore/compartment interface. In order to reduce the simulation time, all simulations were computed in two dimensions with a symmetry axis centered inside the pore and perpendicular to the membrane surface. Any results reported were obtained using a temperature of 21°C, a KCl concentration of 0.4 M, and an applied voltage of 200 mV.

All results were steady-state solutions of the Poisson-Nernst-Planck equations, which involve three different physics models in COMSOL. The first and simplest model to implement is the Poisson equation,

$$\nabla^2 V = \frac{-\rho}{\varepsilon_0 \varepsilon_r} \qquad \text{(S2)}$$

with ε_r as the relative permittivity of water (which we take to be 80) and ρ as the summed charge density of K^+ and Cl^- ions. This equation couples V with the concentration of ions C_i since the space charge density is $\rho = F(C_K - C_{Cl})$, where F is the Faraday constant. The boundary condition used in this model is a zero charge on all surfaces with the exception of setting V = 0 V at the top of the *cis* compartment and V = 200 mV at the bottom of the *trans* compartment. The second physics model used is the Navier-Stokes equation,

$$\rho_w(\mathbf{u}\cdot\vec{\nabla})\mathbf{u} = \eta\nabla^2\mathbf{u} - \vec{\nabla}p + \mathbf{F} \qquad \text{(S3)}$$

where ρ_w is the density of water, ***u*** is the fluid velocity, η is the viscosity of water, p is the pressure, and ***F*** is the sum of all external forces per unit volume. The only external force that is significant in our experiment is the volume electrostatic force due to ionic charge, $\mathbf{F}(r,z) = -\vec{\nabla}V \cdot F(C_K - C_{Cl})$. A no slip boundary condition was enforced in this model at all surfaces. The final physics model employed is a simplified Nernst-Planck equation,

$$\vec{\nabla}\cdot(D\vec{\nabla}C_i + z_i\mu F C_i\vec{\nabla}V) - \mathbf{u}\cdot\vec{\nabla}C_i = 0 \qquad \text{(S4)}$$

where D is the diffusion coefficient (which we estimate as 2 x 10^{-9} cm^2/s for K^+ and Cl^-), z_i is the charge number of each ionic species, and μ is the electrophoretic mobility defined using the Einstein-Smoluchowski relation $\mu = D/k_bT$. This equation has been simplified by assuming that our fluid is incompressible ($\vec{\nabla}\cdot\mathbf{u} = 0$) and enforcing a steady-state solution ($\partial C_i/\partial t = 0$). The boundary conditions given for this model are a salt concentration of 0.4 M KCl at the top cap of the *cis* chamber and bottom cap of the *trans* chamber, and no flux of ions at any surface in the geometry. This model incorporates all forms of motion for the ionic species in a nanopore experiment: diffusion, electro-migration, and convection.

SM-8: *Agarose gel of DNA samples*

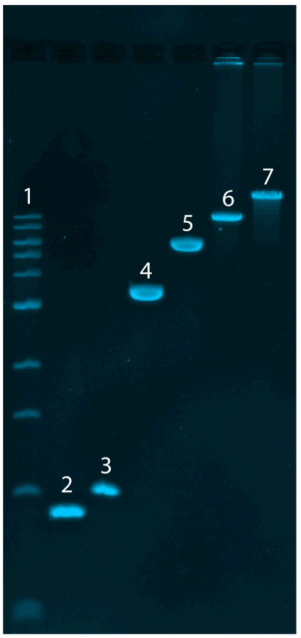

FIGURE S5 An agarose gel of DNA lengths 1 kbp – 20 kbp. To ensure that our long DNA samples ($N > 1$ kbp) are pure, we prepared and a 1% agarose gel with a 1 kb ladder as a control and ran it for 100 minutes at 100 V. After staining the gel with ethidium bromide for ~30 min, it was then imaged. Each sample is labeled in the gel as follows: (1) 1 kb ladder, (2) 900 bp (not used in experiments), (3) 1 kbp, (4) 3.5 kbp, (5) 6 kbp, (6) 10 kbp, (7) 20 kbp. As observed in the gel results, each DNA sample shows one clear band that corresponds to the correct length according to the 1 kb ladder.

SM-9: *Transport Time vs. DNA Length Studies*

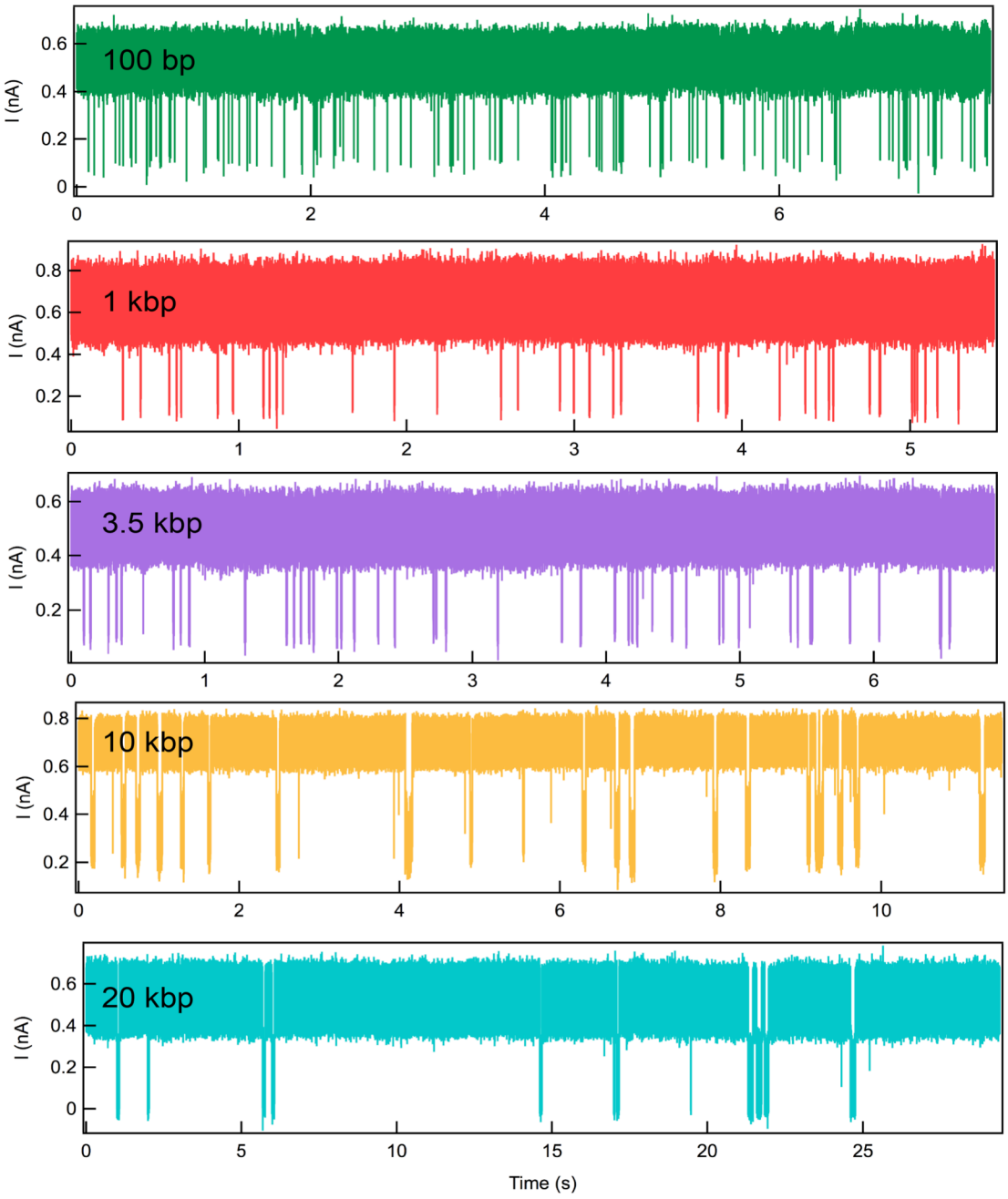

FIGURE S6 Continuous current traces for 100 bp, 1 kbp, 3.5 kbp, 10 kbp and 20 kbp DNA for nanopores with d = 2.8-3.0 nm. The mean open pore current ranges from 0.5-0.7 nA due to small variances in membrane thickness. Despite the open pore current being stable, it would occasionally increase (i.e., < 10%) over the course of an experiment due to solution evaporation or pore expansion, which required the vast majority of datasets to be collected in experiments of less than 20 minutes in duration. Longer DNA lengths had lower sample concentrations to avoid the clogging of our pores due to the longer transport times required for translocation.

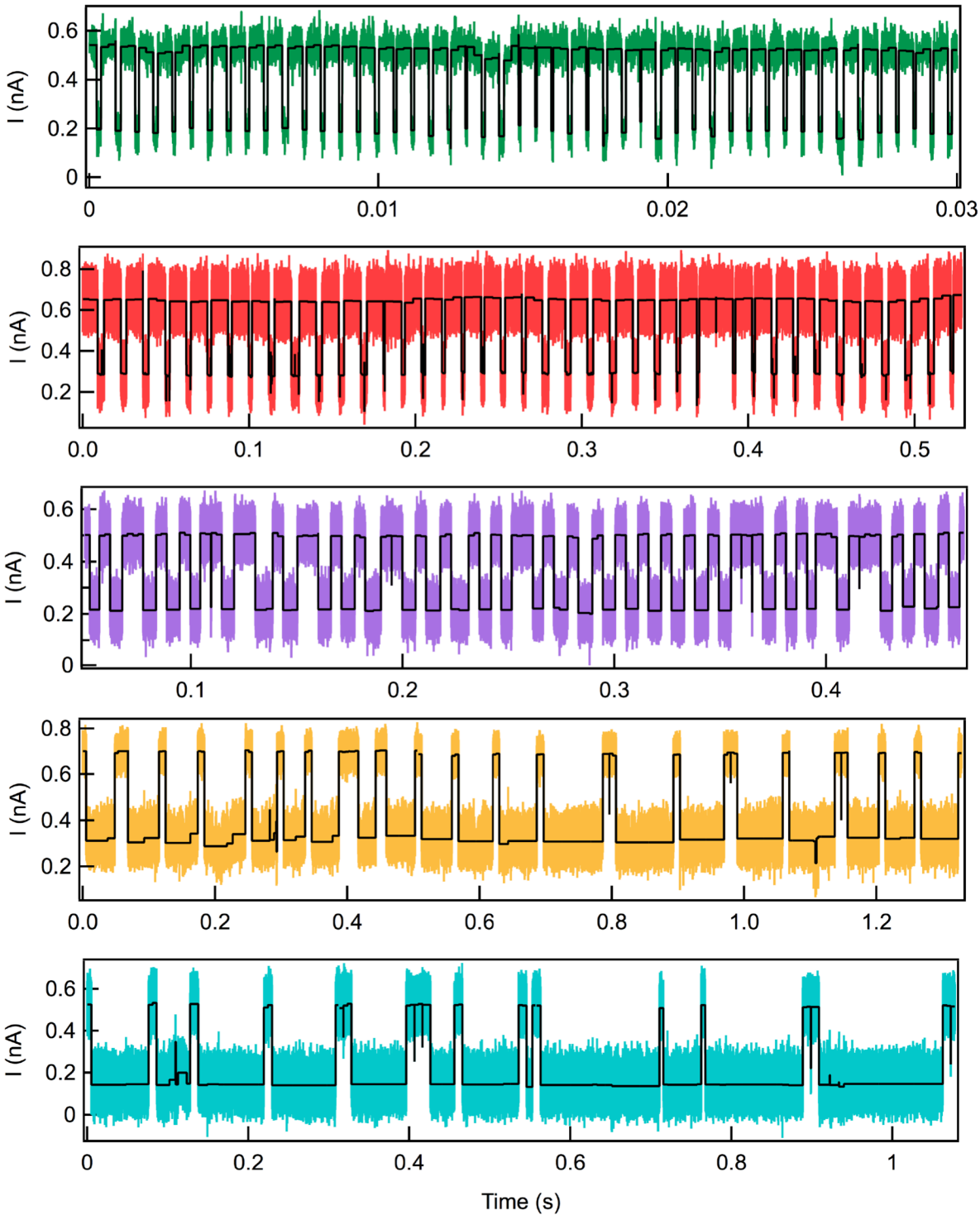

FIGURE S7 Concatenated current traces of consecutive events for the data shown in Figure S6 overlaid with analysis fits obtained by OpenNanopore software. The traces show that we detect a vast majority of translocations with a single current blockade level with the occasional fast collision or multi-level translocation.

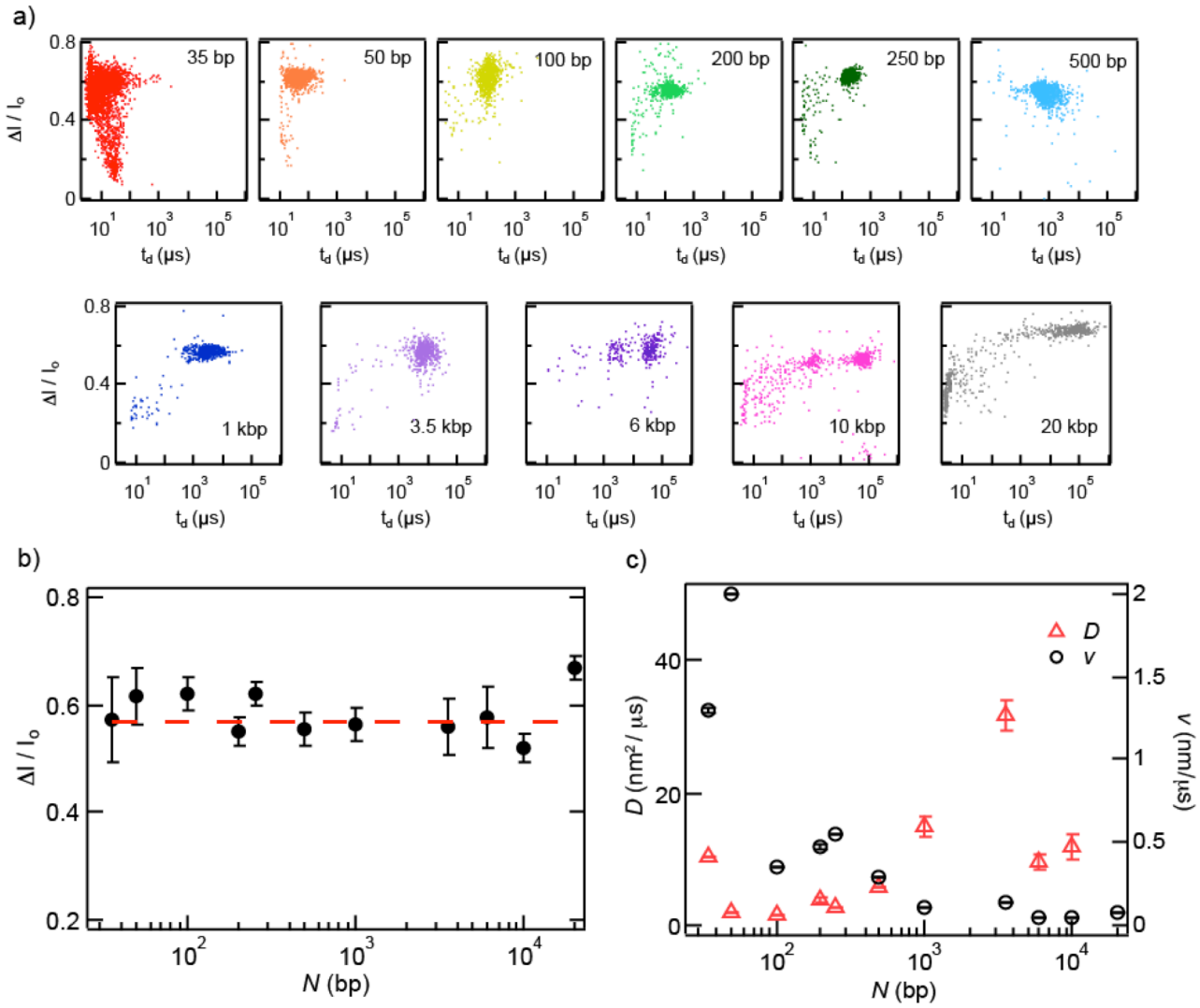

FIGURE S8 (***a***) Scatter plots of $\Delta I/I_o$ vs. t_d for 11 DNA fragments through different nanopores, all in the range of d = 2.8-3.0 nm. Single event populations are seen for $N < 6$ kbp, while additional populations are seen for DNA lengths $N > 6$ kbp. The fast ($t_d < 100$ μs) events for long DNA are attributed to DNA collisions with the pore, caused by an increased barrier for a long DNA end to find the pore mouth. Further, we speculate that the additional slow population that forms for $N > 6$ kbp is due to DNA shearing or some other disruptive process by the nanopore. Contamination was ruled out by observing a single band in the gel electrophoresis for these fragments (see **Fig. S5**), and we do not have any proof for our claim of DNA shearing (apart from the faster timescale of these events than expected). Since this intermediate population contains a very small minority of the total events, we claim that the slowest population corresponds to DNA translocations. (***b***) A plot of $\Delta I/I_o$ vs. N for the pores used in (**a**), demonstrating the similar diameters used in the experiments. When fitting to a horizontal line, we find a mean $\langle \Delta I/I_o \rangle$ value of 0.57. (***c***) A plot of v vs. N shows a decreasing velocity with contour length. However, in the plot of D vs. N no definite trend is discernable. The anomalously high value of D for N = 20 kbp (D = 270 nm^2 μs^{-1}) is not shown in the plot in order to show the trend for most of the other DNA lengths.

TABLE S1. Dwell Time vs. DNA Length Data

***N* (bp)**	n_{total}	t_d *(± err)*
35	3315	17 ± 1 μs
50	2121	49 ± 2 μs
100	911	135 ± 8 μs
200	679	153 ± 4 μs
250	806	169 ± 3 μs
500	2593	890 ± 20 μs
1000	552	3.62 ± 0.14 ms
3500	590	8.51 ± 0.25 ms
6000	283	39.1 ± 2.2 ms
10,000	424	67 ± 2 ms
20,000	419	80 ± 4 ms

Supporting References

1. Kim, M. J., M. Wanunu, D. C. Bell, and A. Meller. 2006. Rapid fabrication of uniformly sized nanopores and nanopore arrays for parallel DNA analysis. Adv. Mater. 18:3149-3155.
2. Kim, M. J., B. McNally, K. Murata, and A. Meller. 2007. Characteristics of solid-state nanometre pores fabricated using a transmission electron microscope. Nanotechnology. 18:205302.
3. Smeets, R. M. M., U. F. Keyser, N. H. Dekker, and C. Dekker. 2008. Noise in solid-state nanopores. P. Natl. Acad. Sci. USA. 105:417-421.
4. Tabard-Cossa, V., D. Trivedi, M. Wiggin, N. N. Jetha, and A. Marziali. 2007. Noise analysis and reduction in solid-state nanopores. Nanotechnology. 18:305505.
5. Wanunu, M., T. Dadosh, V. Ray, J. M. Jin, L. McReynolds, and M. Drndic. 2010. Rapid electronic detection of probe-specific microRNAs using thin nanopore sensors. Nat. Nanotechnol. 5:807-814.
6. Hall, J. E. 1975. Access resistance of a small circular pore. J. Gen. Physiol. 66:531-532.
7. Vodyanoy, I., and S. M. Bezrukov. 1992. Sizing of an ion pore by access resistance measurements. Biophys. J. 62:10-11.
8. Li, G., and J. X. Tang. 2004. Diffusion of actin filaments within a thin layer between two walls. Phys. Rev. E. 69:061921.
9. McMullen, A., H. W. de Haan, J. X. Tang, and D. Stein. 2014. Stiff filamentous virus translocations through solid-state nanopores. Nature Communications. 5.